# Quasicrystalline and Dynamic Planforms in Nonlinear Optics

Len M. Pismen and Boris Y. Rubinstein,
*Department of Chemical Engineering* and
*Minerva Center for Research in Nonlinear Phenomena,*
*Technion - I.I.T., Technion City, Haifa 32 000, Israel*

**Abstract**

A variety of stationary and wave patterns that show a complicated spatial structure but are ordered in the Fourier space can be constructed by considering interaction of non-collinear modes near a symmetry breaking bifurcation point. The planform selection is particularly rich in the presence of resonant (phase-dependent) interactions among degenerate modes. We consider the problem of pattern selection for two optical systems: a cavity with two nonlinear elements and a cavity with a rotated optical field. Complex quasicrystalline patterns sustained by resonant interactions arise under conditions when wave and Turing modes are excited simultaneously. The excited patterns may be saturated even by the action of quadratic (three-wave) interactions only, and may exhibit periodic amplitude modulation on a slow time scale.

PACS 42.65.Sf

## 1 Introduction: complex order

Spontaneous symmetry breaking and pattern formation is a universal phenomenon observed in a wide variety of non-equilibrium systems [1, 2]. Most commonly, patterns have a simple basic structure, usually stripes or hexagons, which is distorted on a long scale, so that the pattern has disordered local orientations, and contains various defects – domain walls, dislocations or disclinations. *Complexity* of patterns is usually understood in the sense of disorder; this is a fascinating but *uncontrollable* kind of complexity.

A rarer kind of complexity is *complex order*: a well-controlled structure ordered in a non-trivial way. *Quasicrystalline* patterns belong to this variety: they have a complicated spatial structure that never repeats itself, but are well ordered in the Fourier space. In principle, constructing such patterns is easy: in two dimensions they can be formed just by superposing four or more non-collinear modes. Near a symmetry-breaking transition from a homogeneous to a patterned or crystalline state (in both equilibrium and non-equilibrium systems) these modes appear formally as degenerate neutrally stable eigenmodes of linearized macroscopic equations, and may admit, in various contexts, different physical interpretations, e.g. density waves in the equilibrium theory [3].

Since a symmetry-breaking transition in an isotropic system implies a preferred wavelength but no preferred direction, an indefinite number of modes may be excited, with the wave vectors $\mathbf{k}_j$ having the same absolute value but arbitrary directed. The emerging pattern or crystalline structure is selected by nonlinear interactions. For stationary (Turing) patterns, lowest-order triplet interactions among modes forming an equilateral triangle are prevalent sufficiently close to a symmetry-breaking transition (unless forbidden by symmetry). These interactions are

*resonant*, i.e. phase-dependent. The phases of the interacting modes always become locked in such a way that the interaction is destabilizing [4], which is responsible for the subcritical (first-order) character of the transition. In a two-dimensional setting (most common in non-equilibrium systems), triplet interactions favor a hexagonal pattern, which is selected, in a generic case, sufficiently close to the bifurcation point.

It turned out to be not easy to overcome the boring pervasiveness of hexagons. A possible source of quasicrystalline patterns is a superposition of two resonant triplets [5]. This pattern can be, however, stabilized only by quadruplet interactions which strongly inhibit multimode patterns because of the occurrence of small angles between the modes. Generally, we expect that non-resonant quadruplet interaction coefficients (involving pairs of modes and their complex conjugates) smoothly depend on the angle between the modes, and therefore interactions at a small angle do not differ very much from interactions at zero angle. The self-interaction coefficient is, for combinatorial reasons, exactly one-half the interaction coefficient of two modes at zero angle, and therefore waves at small angles tend to be mutually damping. Quasicrystalline patterns of Turing type were, however, observed in experiments with parametric excitation of surface waves (Faraday instability) [6, 7]. Conditions suitable for formation of quasicrystalline Turing patterns were detected by the analysis of model equations [8] as well as of amplitude equations of Faraday instability [9]. Patterns formed by two resonant triplets were shown to be one of possible states of Marangoni convection in a layer with a deformable interface [10].

In the case when a symmetry-breaking transition leads to wave patterns, triplet interactions are forbidden. The lowest-order quadruplet interactions are usually non-resonant, although resonance is possible among non-collinear standing waves [11]. Quasicrystalline wave patterns are possible in principle [11] but again are, apparently, rather rare, and not easy to locate because of technical difficulties in evaluation of mode interaction coefficients. Most commonly, wave patterns (as well as Turing patterns in the presence of symmetry to inversion of the order parameter) contain one or two basic modes forming, respectively, a striped or square pattern.

Nonlinear optics provides more possibilities for formation of complex patterns than more conventional chemical or convective systems. A sure recipe for creating a quasicrystal is *rotation* of the optical field in a nonlinear cavity [12] –[16]. The number of modes is dictated then by the rotation angle. If it is commensurate with $2\pi$, so that $\Delta = 2\pi n/N$ (where $n$ and $N$ are integers that do not have common factors), the basic planform is a rotationally invariant combination of $N$ or $N/2$ plane waves (respectively, for $N$ odd or even) which yields a quasicrystalline pattern at $N = 5$, 7, or more.

Further possibilities arise in optical systems because of a relative ease of arranging a degenerate bifurcation of modes with different wavelengths. Recent experiments by the Florence group [15, 16] demonstrated simultaneous excitation of phase-locked families with different wavenumbers, leading to more complicated quasicrystalline patterns. We shall consider this system in detail in Section 3, emphasizing resonant interaction among Turing and wave modes.

The degeneracy may also help to enhance complexity in "natural" patterns where the symmetry is not imposed externally but is selected by nonlinear interactions. In fact, presence of several minima strongly affects the pattern even when the levels are not degenerate (see Section 4.2). An example of selection of a quasicrystalline pattern in a feedback cavity has been recently demonstrated analytically and numerically [17]. We shall consider in Section 4 a cavity with two nonlinear optical elements [18] which can provide a variety of easily switchable quasicrystalline patterns.

Complex order may mean not only spatial but *temporal* complexity. Patterns involving resonant interactions are likely to exhibit complex dynamics of amplitude modulation on a slow time scale due to intermittent phase locking. In this way, one arrives at a dynamic pattern with

ever changing appearance but a permanent composition of the Fourier spectrum; examples are given in Section 3.3 and 4.2. We shall emphasize resonant triplet interactions among Turing and wave modes as a source of dynamic complexity. Unlike purely Turing triplets, these interactions may stabilize a pattern either statically or dynamically within a wide parametric range.

# 2 Amplitude equations and pattern selection

## 2.1 Multiscale expansion

The standard method for the analysis of pattern selection near a symmetry-breaking bifurcation is *multiscale expansion*. The method is well formalized, and *Mathematica*-based software is now available [19, 20]. One can take as a starting point a general system written in an operator form

$$\mathcal{F}(\nabla, \partial/\partial t, \mathbf{u}(\mathbf{r}, t, \mathbf{R}), \mathbf{R}) = 0, \tag{1}$$

where $\mathbf{u}$ is an arrays of state variables, dependent on spatial coordinates $\mathbf{r}$ and time $t$, and $\mathbf{R}$ is an array of parameters of the problem. We suppose that Eq. (1) has a homogeneous stationary solution $\mathbf{u} = \mathbf{u}_0(\mathbf{R})$; it is convenient to shift the variables in such a way that $\mathbf{u}_0(\mathbf{R}) = 0$. Picking a certain set of parameters $\mathbf{R}_0$, we expand both the variables and parameters in powers of a dummy small parameter $\epsilon$:

$$\mathbf{u} = \epsilon\mathbf{u}_1 + \epsilon^2\mathbf{u}_2 + \dots, \quad \mathbf{R} = \mathbf{R}_0 + \epsilon\mathbf{R}_1 + \epsilon^2\mathbf{R}_2 + \dots. \tag{2}$$

We also introduce a hierarchy of time scales:

$$\partial/\partial t = \partial/\partial t_0 + \epsilon\partial/\partial t_1 + \epsilon^2\partial/\partial t_2 + \dots, \tag{3}$$

and expand Eq. (1) in Taylor series. The spatial derivative $\nabla$ may be expanded in the same way to describe modulation of a pattern on a long scale but we shall not be concerned with this here.

The first-order equation contains a matrix $\mathcal{F}_\mathbf{u}$ which is the linearization of $\mathcal{F}$ with respect to the state variables:

$$\mathcal{F}_\mathbf{u}(\nabla_0, \partial/\partial t_0, \mathbf{u}_0, \mathbf{R}_0)\mathbf{u}_1 = 0. \tag{4}$$

Using here $\mathbf{u}_1 = \mathbf{U}\exp(\lambda t + i\mathbf{k}\cdot\mathbf{r})$ leads to an eigenvalue problem

$$\mathcal{F}_\mathbf{u}(ik, \lambda, \mathbf{u}_0, \mathbf{R}_0)\mathbf{U} = 0. \tag{5}$$

We suppose here that the system is isotropic, and therefore the spectrum depends only on the wavenumber $k = |\mathbf{k}|$ but not on the direction of the wave vector. $\mathbf{R}_0$ is a symmetry-breaking bifurcation point, and $k_0$ is the wavenumber of the emerging pattern if the leading eigenvalue $\lambda(k_0, \mathbf{R}_0)$ of $\mathcal{F}_\mathbf{u}$, i.e. that with the largest real part, satisfies Re $\lambda(k, \mathbf{R}_0) = 0$, Re $\partial\lambda(k, \mathbf{R}_0)/\partial k = 0$ at $k = k_0$. It is often convenient to draw a *neutral curve* $R(k)$, where $R$ is the value of one of parameters determined by the condition Re $\lambda(k, R) = 0$. The bifurcation point $R = R_0$ (at all other parameters fixed) is found as the absolute minimum of the neutral curve.

Due to the isotropy, the bifurcation is always degenerate. An additional "accidental" degeneracy occurs when two minima of the neutral curve are equal (generally, the locus of a degenerate bifurcation is a codimension two hypersurface in the parametric space $\mathbf{R}$). The solution of Eq. (4) is expressed as

$$\mathbf{u}_1 = \sum a_j(t_1, t_2, \dots)\mathbf{U}_j \exp(i\mathbf{k}_j\cdot\mathbf{r} + i\omega_j t_0) + c.c., \tag{6}$$

where $a_j$ are as yet indefinite amplitudes which may vary on a slower time scale, and $\omega_j$ =Im $\lambda_j$; $\omega_j = 0$ for a Turing mode, and $\omega_j \neq 0$ for a wave mode. This expression may contain an indefinite number of modes with $\mathbf{k}_j$ directed in a different way, but $\mathbf{U}_j$, $\omega_j$ are distinct only for "accidentally" degenerate modes.

In the consequent orders we arrive at the equations of the form:

$$\mathcal{F}_{\mathbf{u}}(\nabla_0, \partial/\partial t_0, \mathbf{u}_0, \mathbf{R}_0)\mathbf{u}_n = \mathbf{g}_n, \tag{7}$$

where $\mathbf{g}_n$ denotes the $n$-th order inhomogeneity dependent on the amplitudes $a_j$. Amplitude equations are obtained as solvability conditions of Eq. (7), *i.e.* conditions of orthogonality of the inhomogeneity to all eigenfunctions of the adjoint linear problem. In the second order, a nontrivial solvability condition is obtained when the quadratic term (a product of two eigenfunctions, say, $\psi_i$ and $\psi_j$) is *in resonance* with another eigenmode, say, $\psi_l$. This requires that the frequencies and wavenumbers of the three modes involved satisfy the conditions

$$\mathbf{k}_i + \mathbf{k}_j + \mathbf{k}_l = 0, \quad \omega_i + \omega_j + \omega_l = 0. \tag{8}$$

A resonant triplet may involve either three Turing modes or two wave modes with identical frequencies and one Turing mode. The amplitude equations obtained in this order have a general form

$$\dot{a}_l = \mu_l a_l + \nu_{ijl} a_i^* a_j^*, \tag{9}$$

where $\mu_l$ are linear growth coefficients dependent on first-order parametric deviations $\mathbf{R}_1$, $\nu_{ijl}$ are mode interaction coefficients, dot denotes the derivative with respect to the slow time variable $t_1$, and $*$ denotes a complex conjugate. It may be possible to confine the dynamics to a small-amplitude region by combining slightly subcritical and slightly supercritical modes, if the nonlinear terms also act in a mutually contradictory way; an example of such behavior is given below. If these conditions are not met, the amplitudes may be stabilized at higher levels by quadruplet interactions that involve terms cubic in amplitudes, and appear in the next order of the expansion.

### 2.2 Wave–Turing resonance

The simplest wave and Turing resonant structure includes two wave modes with a wavenumber $k$ and amplitudes $b, c$, and one Turing mode with a wavenumber $Q$ and an amplitude $a$; both $k$ and $Q \leq 2k$ should correspond to accidentally degenerate minima of the respective neutral curves. The Fourier space structure is an isosceles triangle. The general form of amplitude equations is

$$\begin{aligned} \dot{a} &= \mu_s a + \nu_s b c^*, \\ \dot{b} &= \mu_w b + \nu_w a c, \\ \dot{c} &= \mu_w c + \nu_w a^* b, \end{aligned} \tag{10}$$

where $\mu_s$ and $\nu_s$ are real, while $\mu_w$ and $\nu_w$ are complex. The imaginary part of $\mu_w$ can be absorbed in frequency, so this parameter will be also viewed as real.

It is advantageous to use the polar representation of the complex amplitudes,

$$a = \rho_a e^{i\theta_a}, \; b = \rho_b e^{i\theta_b}, \; c = \rho_c e^{i\theta_c}. \tag{11}$$

Then Eqs. (10) is reduced to the following system of four real equations including a single phase combination $\theta = \theta_a + \theta_c - \theta_b$:

$$\dot{\rho}_a = \mu_s \rho_a + \nu_s \rho_b \rho_c \cos\theta,$$

$$\begin{aligned}
\dot\rho_b &= \mu_w\rho_b + \nu\rho_a\rho_c\cos(\theta-\alpha),\\
\dot\rho_c &= \mu_w\rho_c + \nu\rho_a\rho_b\cos(\theta+\alpha),\\
\dot\theta &= -\nu_s\frac{\rho_b\rho_c}{\rho_a}\sin\theta - \nu\frac{\rho_a\rho_b}{\rho_c}\sin(\theta+\alpha) - \nu\frac{\rho_a\rho_c}{\rho_b}\sin(\theta-\alpha),
\end{aligned} \tag{12}$$

where we have set $\nu_w = \nu e^{-i\alpha}$.

The stationary values of the amplitudes $\rho_a, \rho_b, \rho_c$ are

$$\rho_a = \frac{\mu_w}{\nu\sqrt{\cos(\theta-\alpha)\cos(\theta+\alpha)}},\quad \rho_{b,c} = \sqrt{\frac{\mu_s\mu_w}{\nu\nu_s\cos(\theta\pm\alpha)\cos\theta}}. \tag{13}$$

The stationary value of the composite phase $\theta$ verifies the equation

$$\tan\theta + \frac{\mu\sin 2\theta}{\cos(\theta-\alpha)\cos(\theta+\alpha)} = 0, \tag{14}$$

where $\mu = \mu_w/\mu_s$. A simple solution of this equation satisfies $\sin\theta = 0$, yielding $\theta = \pi$ at $\mu_s\nu_s > 0$ and $\mu_w\cos\alpha > 0$, and $\theta = 0$ for the opposite sign of these products. This is a symmetric solution with equal amplitudes of the wave modes: $\rho_b = \rho_c = \sqrt{\mu_s\mu_w/(\nu\nu_s\cos\alpha)}$. The stability conditions of the symmetric solution are

$$\mu_w > 0,\quad \frac{\pi}{4} < \alpha < \frac{3\pi}{4},\quad -1/4 < \mu < -\frac{1}{2}\cos^2\alpha. \tag{15}$$

At $\mu_w = 0$ the symmetric solution merges with the trivial solution $\rho_a = \rho_b = \rho_c = 0$; $\mu = -1/4$ is the locus of a supercritical Hopf bifurcation, and $\mu = -\frac{1}{2}\cos^2\alpha$ corresponds to a pitchfork bifurcation to a pair of asymmetric solutions, which is also supercritical at $\mu > -\frac{1}{4}$.

The composite phase of an asymmetric solution verifies the relation

$$\cos^2\theta = \frac{\sin^2\alpha}{1+2\mu}. \tag{16}$$

It is immediately seen that the solution exists provided $\mu \geq -\frac{1}{2}\cos^2\alpha$. It is required for positiveness of the amplitudes that $\cos(\theta-\alpha)\cos(\theta+\alpha) > 0$. This inequality can be rewritten in the form $\mu\sin^2\alpha < 0$, and hence, $\mu < 0$. The two asymmetric solutions are transformed one to the other by interchanging the amplitudes of the wave modes.

At still higher values of $\mu$, the asymmetric solutions undergo a supercritical Hopf bifurcation. The bifurcation locus in the plane $(\alpha, \mu)$ is given implicitly by the relation

$$\begin{aligned}
-(1+4\mu)(1+5\mu+8\mu^2)\sin^4\alpha + 3(4+7\mu+4\mu^2)(2\mu+\cos^2\alpha)^2 +\\
[3+8\mu(\mu+2)(1+2\mu)](2\mu+\cos^2\alpha)\sin^2\alpha = 0.
\end{aligned} \tag{17}$$

The additional stability condition is $\mu_s < 0$. The resulting bifurcation diagram in the plane $\mu, \alpha$ is presented in Fig. 1. The picture in the range $\pi/2 < \alpha \leq \pi$ is symmetric relative to the axis $\alpha = \pi/2$.

A pair of asymmetric periodic solutions further merges into a symmetric attractor as a result of a homoclinic bifurcation. We were unable to determine the locus of this bifurcation exactly because of a very complicated dynamics in the vicinity of a saddle point in the four-dimensional phase space. This is a saddle-focus with two-dimensional stable and unstable manifolds, both oscillatory. Our numerical estimates suggest that the homoclinic boundary is roughly defined by the relation $\mu = -\pi\alpha$ (marked by a dashed line in Fig. 1). On the other side of this boundary, the dynamics is apt to be chaotic. A period doubling of the symmetric periodic

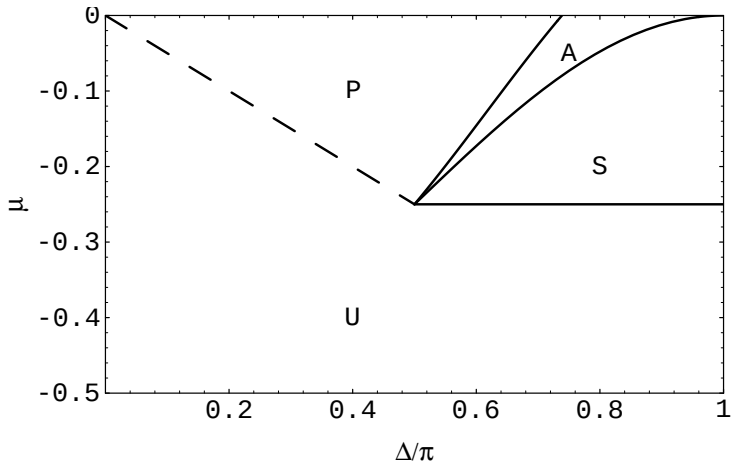


Figure 1: Bifurcation diagram of Eq. (12) in the parametric plane ($\alpha$, $\mu$). Letters S and A denote the regions of stable stationary symmetric and asymmetric solutions; P stands for a pair of periodic solutions, and U for a symmetric periodic solution or other symmetric dynamic attractor. The dashed line shows an approximate location of the homoclinic bifurcation.

solution observed close to the double zero singularity at $\mu = 1/4,\ \alpha = \pi/4$ is illustrated in Fig. 2.

While an asymmetric periodic solution cannot transcend the saddle point, there are no apriori limits on the amplitude of symmetric oscillations, which tends to grow as $\mu$ becomes more negative. Confinement in the small-amplitude region by quadratic interactions is only possible when the Turing mode is subcritical and the wave mode is supercritical but not too strongly. When runaway to large amplitudes is observed in Eqs. (12), the actual pattern may be stabilized by non-resonant quadruplet interactions.

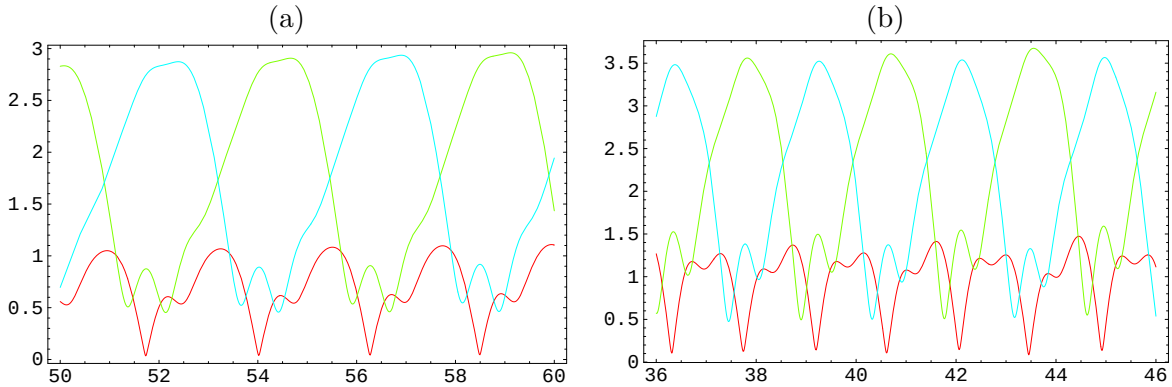


Figure 2: Amplitude oscillations at $\alpha = 0.22\pi$ and $\mu = -0.23$ (a), $\mu = 0.28$ (b). Oscillations of the Turing mode have the smallest amplitude.

# 3 Optical cavity with a rotated beam

## 3.1 Basic Equations

Our first example is an optical cavity with a rotated beam. The successive transformations of the complex envelope of the electric field $E_i(\mathbf{r})$ of a light beam in a nonlinear optical cavity with a rotated beam include three stages: (a) point transformation in the nonlinear medium, adding a phase shift dependent on the transverse coordinate $\mathbf{r}$; (b) diffraction in the empty part of the cavity, described by a linear operator $\mathcal{D}$, and (c) rotation of the image, described by an operator $\mathcal{J}(\Delta)$.

The first transformation takes place in a thin slice of a nonlinear Kerr-type medium, which is assumed to be uniform in the longitudinal direction. The field is transformed as

$$E_i(\mathbf{r}) \to R_1 E_i(\mathbf{r}) \exp(-i\chi(\mathbf{r}) + i\Omega), \tag{18}$$

where $\chi$ is the normalized refractive index of the medium, $\Omega$ is a constant phase shift and $R_1$ is the attenuation coefficient due to the absorption in the layer.

Propagation and diffraction of the beam in the free part of the cavity is described by the diffractional transform $\mathcal{D}(z)$ which is obtained in the paraxial approximation [21] as the resolvent of the parabolic equation

$$iE_z = \nabla^2 E. \tag{19}$$

Here the coordinate $z$ in the direction of propagation is scaled by the length $L$ of the diffractional path, and the transverse coordinates, by the diffractional length $\sqrt{L\lambda}$, where $\lambda$ is the wavelength; $\nabla^2$ denotes the two-dimensional transverse Laplacian. Formally, one can write $\mathcal{D}(z) = \exp(-iz\nabla^2)$, so that $\mathcal{D}(z) = \exp(izk^2)$ when it operates upon a Fourier mode with a transverse wave number $k$.

Before closing the loop, the image is rotated by a certain angle $\Delta$. The rotation is described by the operator

$$\mathcal{J}(\Delta):\ \mathcal{J}(\Delta)\{r,\phi\} = \{r, \phi + \Delta\}. \tag{20}$$

The resulting output field $E_o$ can be written as

$$E_o(\mathbf{r}) = \mathcal{J}(\Delta) R \mathcal{D}(1) E_i(\mathbf{r}) \exp[-i\chi(\mathbf{r}) + i\Omega], \tag{21}$$

where the attenuation coefficient $R$ lumps all losses during a single round-trip.

The model of material dynamics can be written, assuming a Kerr-type nonlinearity, in the dimensionless form [22]

$$\dot{\chi} = \delta^2 \nabla^2 \chi - \chi - \kappa_1 |E_o\left(\chi(\mathbf{r})\right)|^2, \tag{22}$$

The material response time is taken as the time scale; $\delta$ is the ratio of the photocarrier diffusion length to the diffraction length. Although typically $\delta \ll 1$, the thin sample approximation can be retained, provided the diffusional length far exceeds $\lambda$, so that longitudinal wavelength scale grating is washed out by diffusion. Then Eq. (22) retains only the transverse Laplacian $\nabla^2$. Dynamics of the refractive index modulation $\chi$ depends on the strength of the nonlinearity $\kappa_1$, which is positive for a defocusing medium.

We shall assume that the material response time is much larger than the round-trip time in the cavity. Under these conditions, the electric field envelope is quasistationary, being slaved to the material variable. Combining the cavity transform Eq. (21) with the appropriate feedback conditions allows then to express $E(\mathbf{r})$ as a nonlinear functional of the material field $\chi(\mathbf{r})$. Now Eq. (22) is rewritten as

$$\dot{\chi} = \delta^2 \nabla^2 \chi - \chi - \kappa \mathcal{J}(\Delta) I |\exp(-i\nabla^2) \exp(-i\chi)|^2, \tag{23}$$

where $I$ denotes the input beam intensity and $\kappa = \kappa_1 R^2$.

Equation (23) always has a stationary homogeneous solution $\chi_0 = -\kappa I$ which, however, may lose stability when the input intensity exceeds a certain critical level. The critical intensity, as well as the preferred transverse wavelength of the emerging pattern is determined by the linear stability analysis of the homogeneous solution.

### 3.2 Linear Analysis

The standard procedure of linear analysis involves testing stability to arbitrary infinitesimal perturbations, usually plane waves. The rotation of the optical field mixes different Fourier modes, and thereby limits the choice of basis functions. Proceeding in a standard way, we set $\chi = \chi_0 + \epsilon\chi_1(\mathbf{r})$, where $\epsilon \ll 1$, and linearize Eq. (23) presenting the linear term $\chi_1$ as the sum of $N$ modes with the wave vectors $\mathbf{q}_i$ $(i = 1, 2, \ldots, N)$ equispaced by the angle $\Delta$, and their complex conjugates:

$$\chi_1 = \sum_{j=1}^{N} a_j \exp(i\mathbf{q}_j\mathbf{r} + \lambda t) + c.c. \tag{24}$$

The linear eigenvalue problem then reads:

$$\mathcal{L}\chi_1 \equiv \left[\lambda + 1 + \delta^2 q^2 + 2\kappa I \sin(q^2)\mathcal{J}(\Delta)\right]\chi_1 = 0. \tag{25}$$

Because the action of the rotation operator has the form $\mathcal{J}(\Delta)\mathbf{q}_i = \mathbf{q}_{i+1}$, the term $\mathcal{J}(\Delta)\chi_1$ is expressed as

$$\mathcal{J}(\Delta)\chi_1 = \sum_{j=1}^{N} a_j \exp(i\mathbf{q}_{j+1}\mathbf{r} + \lambda t) + c.c., \tag{26}$$

where the indices are cyclic modulo $N$. The amplitude vector $\mathbf{a}$ comprised of the amplitudes $a_j$ satisfies the eigenvalue problem $\mathbf{Ma} = \lambda\mathbf{a}$ with a circulant matrix $\mathbf{M}$, such that $\mathbf{M}_{i,i} = -(1+\delta^2 q^2)$ and $\mathbf{M}_{i,i-1} = -2\kappa I \sin q^2$; all other elements of $\mathbf{M}$ are zeroes. The set of eigenvalues of the matrix $\mathbf{M}$ is

$$\lambda_j = -(1 + \delta^2 q^2 + 2\kappa I r_j^{N-1} \sin q^2). \tag{27}$$

The components $\mathbf{U}_{j,k}$ of the corresponding eigenvectors $\mathbf{U}_j$ are

$$\mathbf{U}_{j,k} = r_j^{k-1} \equiv e^{2\pi i j/N}, \quad j = 1, \ldots, N, \tag{28}$$

where $r_j$ denotes the $j$-th root of unity of $N$th degree.

The basic state $\chi_0$ loses stability at $\mathrm{Re}\,\lambda_j = 0$, which determines the location of the neutral curve:

$$I = -\frac{1 + \delta^2 q^2}{2\kappa \sin q^2 \cos(\Delta j)}. \tag{29}$$

The positive branches of this curve give the critical value of the bifurcation parameter $I$ corresponding to excitation of a planform with the wavenumber $q$. The selected type of planform and the wavenumber correspond to the absolute minimum of $I(q)$.

The cases of even and odd values of $N$ should be considered separately, and we restrict ourselves to the more interesting case of odd $N$ which provides a possibility of a resonance among composite modes bifurcating at different wavelengths. The lowest minima of the positive branches of the neutral curve may have close levels. Such minima are reached at $j = (N+1)/2$ and $j = N$, respectively.

For the case $j = N$, the eigenvalue is real, and a composite Turing mode is excited. The neutral curve is given by

$$I = -\frac{1 + \delta^2 q^2}{2\kappa \sin q^2}. \tag{30}$$

In the case $j = (N+1)/2$, the eigenvalue is complex, and the critical value of the bifurcation parameter $I$ is

$$I = \frac{1 + \delta^2 q^2}{2\kappa \cos(\Delta/2) \sin q^2}. \tag{31}$$

The emerging structure can be characterized as a composite *wave* mode with a non-zero frequency $\omega = (1 + \delta^2 q^2) \tan(\Delta/2)$.

In the diffractional limit, $\delta \ll 2\pi/q$, all branches have minima at $q^2 = (2m+1)\pi/2$ with integer $m$. Only first branches which have the lowest minima are relevant for the pattern selection. The wave mode has the lowest minimum at $q = \sqrt{\pi/2}$, while the first positive minimum of the Turing mode is located at $q = \sqrt{3\pi/2}$.

It can be shown that for small odd $N$ the composite Turing mode is most dangerous, while for large $N$ the composite wave mode has the lowest threshold. It is easy to determine the critical value of $N$ when both modes can be excited simultaneously. This value is given by

$$N_{cr} = (1/\pi) \arccos \frac{1 + 2/(\pi\delta^2)}{3 + 2/(\pi\delta^2)}. \tag{32}$$

The calculations using the values of the parameters reported in [14] give the best fit integer value $N = 11$. The first two positive branches of the neutral curve $I(q)$ for the composite wave and Turing modes each comprised of 11 plane wave modes are shown in Fig. 3. Their minima are close to each other, and both may be excited simultaneously.

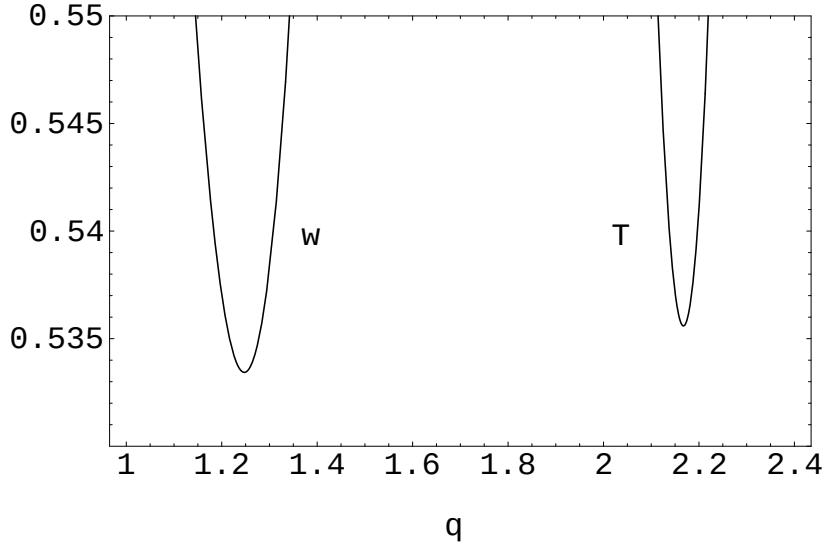


Figure 3: First positive branches of the neutral curves (30), corresponding to a composite Turing mode (T), and (31), corresponding to a composite wave mode (w), for $N = 11$.

### 3.3 Three-mode resonance

A possible resonant structure that may be excited at odd $N$ consists of two composite wave modes with a wavenumber $q$ and one composite Turing mode with the wavenumber $Q = \sqrt{3}q$. The pattern in the Fourier space it is built of $N$ identical isosceles triangles with acute angles equal to $\pi/6$ (and their conjugates produced by rotating the original triangles by $\pi$). The triangles are spaced by the angle $\Delta = 2\pi/N$. Altogether, this resonant planform is built of $3N$ plane wave modes:

$$\chi_1 = \sum_{j=1}^{N} \left\{ a_j e^{i\mathbf{Q}_j\mathbf{r}} + e^{i\omega t}(b_j e^{i\mathbf{q}_j\mathbf{r}} + c_j e^{i\mathbf{k}_j\mathbf{r}}) \right\} + c.c. \ , \tag{33}$$

where $|\mathbf{q}_j| = |\mathbf{k}_j| = |\mathbf{Q}_j|/\sqrt{3}$, and the following relations are satisfied:

$$\mathbf{q}_j - \mathbf{k}_j = \mathbf{Q}_j, \ \ a_j = a, \ \ b_j = (-e^{i\Delta/2})^j b, \ \ c_j = (-e^{i\Delta/2})^j c. \tag{34}$$

The first of these is the resonance condition (8). The relations among the amplitudes of the Fourier modes are imposed by the rotational symmetry, and correspond to the eigenvectors (28).

A snapshot of the pattern defined by Eq. (33) and the corresponding structure in the Fourier space are shown in Fig. 4. The planform has a complicated non- stationary quasicrystalline structure. Since the plane waves comprising the pattern are out of phase by $\Delta/2$, the pattern exhibits rotational motion at each location.

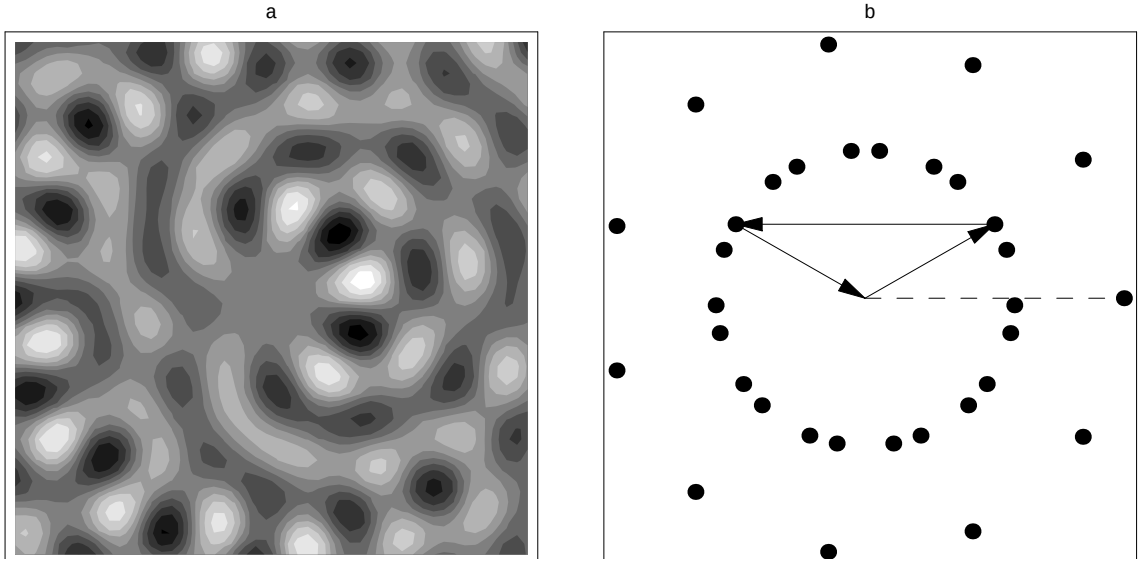


Figure 4: The planform (33) with $N = 11$. (a) A snapshot of a real space (near field) image. (b) The structure in the Fourier space (far field image). The inner circle corresponds to wave modes, and the outer circle, to Turing modes. Complex conjugate modes are omitted. One of the resonant isosceles triangles is shown, and the participating Turing mode is indicated by the dashed line.

The dynamic equations for the amplitudes $a, b$ and $c$ are obtained following the standard procedure outlined in Section 2. Using the relations (34) we arrive after some algebra at the following system of amplitude equations:

$$\dot{a} \ = \ \mu_s a - \nu b c^*,$$

$$\begin{aligned} \dot{b} &= (\mu_w b + \nu a c) e^{-i\Delta/2}, \\ \dot{c} &= (\mu_w c + \nu a^* b) e^{-i\Delta/2}, \end{aligned} \tag{35}$$

where $\nu = \kappa I_0$, $\mu_s = 2\kappa I_{1s}$, and $\mu_w = 2\kappa I_{1w}$; $I_{1s}$ and $I_{1w}$ denote small deviations from the critical value $I_0$ for the Turing (stationary) and wave composite modes, respectively. These deviations may have different signs due to different values of the corresponding minima of the neutral curve. Further on, we choose them to be of the opposite sign. This means that one of the composite modes is subcritical and the other one is supercritical. This case is most interesting, as it allows to prevent both decay to the trivial state and runaway to large amplitudes through the action of quadratic interactions.

Equations (35) are a particular case of Eqs. (10), and are reduced to the latter by replacing $\mu_w \cos(\Delta/2) \to \mu_w$, and setting $\nu_s = \nu$, $\Delta = 2\alpha$. All results of the analysis in Section 2.2 are applicable. At $N = 11$, the small-amplitude dynamics is periodic, as follows from the bifurcation diagram in Fig. 1. The long-time oscillations of the type shown in Fig. 5 modulate the non-stationary quasicrystalline structure shown in Fig. 4. The periodic orbit seen here is rather close to the homoclinic bifurcation discussed in Section 2.2. At a certain moment during the oscillation cycle, two amplitudes become nearly extinct, while the composite phase undergoes sharp oscillations and switches to an alternative level.

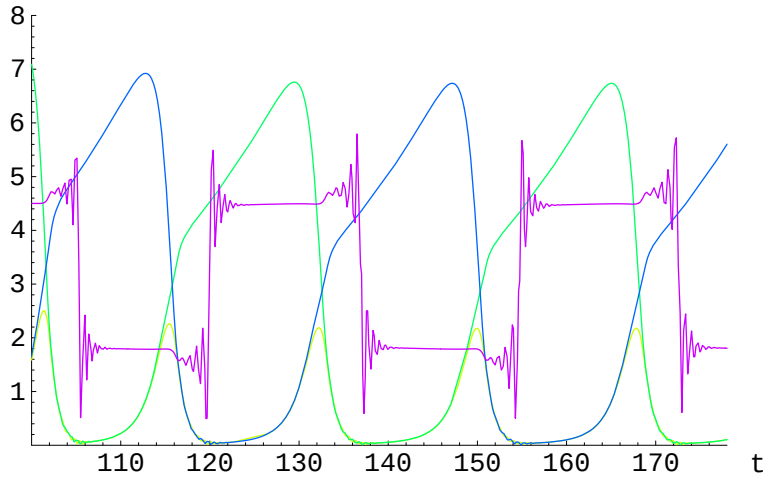


Figure 5: A periodic solution of the system Eq. (35) for $N = 11$ at $\mu_w/\mu_s = -1/20$. The composite phase $\theta$ remains nearly constant during a larger part of each half-period, and undergoes sharp oscillations before and after switching to the alternative level. Oscillations of the two wave modes are identical but shifted by half-a-period. Oscillations of the Turing mode have a smaller amplitude, and a twice shorter period.

### 3.4 Strained resonance

One can also envisage a structure based on a single composite wave mode and a single composite Turing mode. It is clear that, while in this structure all resonant triangles remain isosceles, the acute angles have slightly different values, and the wavelengths must be different from the exact minima of the neutral curve. We call it therefore a *strained* resonance. Excitation of a strained planform is likely because modes at small acute angles are usually damped by quadruplet interactions, and tend to "merge". The smallest angle between two wave modes

involved in the exact resonant planform corresponds to a mismatch between $m\pi/N$ and $n\pi/6$, where $m, n$ are integers, and comes at $N = 11$ to a mere $\pi/66$, i.e. less than $3^\circ$.

Although quadruplet interactions are weaker than triplet ones at small amplitudes, and we do not consider them here explicitly, we may expect that the system might choose to reduce the number of modes and adjust to the resonance by straining the wavelength slightly off the optimal value. The required value can be achieved by reducing the wavenumber of the wave mode from $q$ to $q(1 - \epsilon_N)$, where $\epsilon_N \ll 1$ depends on $N$. The calculation for $N = 11$ gives $\epsilon_{11} \approx 0.048$.

A strained resonant pattern has a simpler structure than the exact resonant planform because it is built up of only $2N$ plane waves, and contains only two independent amplitudes:

$$\chi_1 = \sum_{j=1}^{N} \left[ a_j e^{i\mathbf{Q}_j \mathbf{r}} + b_j e^{i\omega t} e^{i\mathbf{q}_j \mathbf{r}} \right] + c.c. \ , \tag{36}$$

where the amplitudes satisfy the relations (34).

At the first sight, the amplitude equations appear to be more involved in this case, since each elementary wave mode $\mathbf{q}_j$ takes part in two resonant triangles: $\mathbf{Q}_j = \mathbf{q}_j - \mathbf{q}_{j+n}$ and $\mathbf{Q}_{N+j-n} = \mathbf{q}_{N+j-n} - \mathbf{q}_j$. In fact, the dynamic equations can be reduced with the help of the relations (34) to a simple form

$$\begin{aligned} \dot{A} &= \mu_s A + \nu_s |b|^2, \\ \dot{b} &= \mu_w e^{-i\Delta/2} b + \nu_w e^{-i\Delta/2} b (A + A^*). \end{aligned} \tag{37}$$

where $A = a e^{in\Delta/2}$, and

$$\begin{aligned} \nu_s &= (-1)^{n+1} 2\kappa I_0 \sin^2(Q^2/2), \quad \nu_w = (-1)^n 2\kappa I_0 \sin^2(q^2/2), \\ \mu_s &= -2\kappa I_{1s} \sin Q^2, \quad \mu_w = 2\kappa I_{1w} \sin q^2. \end{aligned} \tag{38}$$

The dynamic behavior under conditions of strained resonance is much simpler. One can see that the relevant dynamic variables in Eqs. (37) are the real part of the composite Turing mode $r = \mathrm{Re}\ A$ and the modulus of the wave mode $p = |b|^2$. Transforming to these variables we obtain the system of two real equations only:

$$\begin{aligned} \dot{r} &= \mu_s r + \nu_s p, \\ \dot{p} &= 2p(\mu_w + 2\nu_w r) \cos(\Delta/2). \end{aligned} \tag{39}$$

The stationary solution is

$$r = -\frac{\mu_w}{2\nu_w}, \quad p = \frac{\mu_w \mu_s}{2\nu_w \nu_s}. \tag{40}$$

According to Eq. (38), $\nu_w \nu_s < 0$, and the above solution exists only if $\mu_w \mu_s < 0$. The stability conditions of the solution are $\mu_s < 0,\ \mu_w > 0$, and $\cos(\Delta/2) > 0$. Thus, the stability region is greatly enlarged, compared to the exact resonance, and encompasses now the entire quadrant $\mu < 0,\ 0 < \Delta < \pi$ in Fig. 1, while periodic long-time dynamics is not observed anymore.

### 3.5 Double resonance

Interactions of composite waves are more complicated when $N$ is divisible by 3. In this case, one has to include also additional resonant terms corresponding to interaction of Turing modes

comprising the Turing composite mode. The resonant conditions for these modes have the form $\mathbf{Q}_j + \mathbf{Q}_{j+m} + \mathbf{Q}_{j+2m} = 0$ where $m = N/3$. It must be noted that the resonance involving one Turing and two wave modes becomes in this case exact, *i.e.*, it is excited at the values of wavenumbers corresponding to the minima of the neutral curve.

Repeating the derivation procedure and using the relations (34) we arrive at the system of amplitude equations:

$$\begin{aligned} \dot{A} &= 2\mu_s A + (|b|^2 + A^{2*}), \\ \dot{b} &= be^{-i\Delta/2}[2\mu_w - (A + A^*)], \end{aligned} \tag{41}$$

where $A = a_j e^{im\Delta/2}$, $\mu_s = I_{1s}/I_0$, $\mu_w = I_{1w}/I_0$, and the time variable is rescaled by $\kappa I_0$.

Equations (41) including double resonance differ from Eq. (37) only by the presence of a self-interaction term for the Turing composite mode. This term is destabilizing, and, in the case of pure Turing patterns, one needs to include third-order terms dependent on four-wave interactions to ensure amplitude saturation. We shall see that, due to the quadratic wave-Turing resonance, the pattern can be stabilized in the small-amplitude region. The system, however, still possesses a large-amplitude attractor.

Setting in (41) $A = re^{i\theta}$, $b = pe^{i\tau}$ yields

$$\begin{aligned} \dot{r} &= 2\mu_s r + (p^2 \cos\theta + r^2 \cos 3\theta), \\ \dot{p} &= 2p(\mu_w - r\cos\theta)\cos(\Delta/2), \\ \dot{\theta} &= -(p^2 \sin\theta + r^2 \sin 3\theta)/r. \end{aligned} \tag{42}$$

The phase of the wave mode is irrelevant also in this case, so that the equation for $\tau$ is separated and may be dropped. The phase of the Turing mode relaxes to zero; thus, the stationary solution is

$$\theta = 0,\ r = \mu_w,\ p = -\mu_s\sqrt{-\mu(\mu+2)}, \tag{43}$$

where $\mu = \mu_w/\mu_s$. The solution exists at $\mu_w > 0,\ \mu_s < 0,\ 0 > \mu > -2$. For stability analysis, it is sufficient to consider a simplified system with $\theta = 0$:

$$\begin{aligned} \dot{r} &= 2\mu_s r + p^2 + r^2, \\ \dot{p} &= 2p(\mu_w - r)\cos(\Delta/2). \end{aligned} \tag{44}$$

The trace of the linearized system is $2(\mu_s + \mu_w)$; thus, a Hopf bifurcation takes place at $\mu = -1$. This bifurcation is subcritical. The system always possesses an additional attractor $p \to 0$, $r \to \infty$, and an unstable orbit which exists at $\mu > -1$ bounds the attraction domain of the small-amplitude solution. At $\mu < -1$, all trajectories are attracted to the large-amplitude region, and taking into account higher-order terms is necessary to obtain finite solutions.

# 4 Optical cavity with two nonlinear elements

## 4.1 Basic equations and linear analysis

An optical cavity with two nonlinear elements is sufficiently versatile to generate quasicrystalline symmetry spontaneously, and to display much of the phenomena described in the preceding Section without externally imposed rotation. The system consists of two Kerr slices S1 and S2, a mirror M, and a beam splitter BS coupling the two nonlinear elements (Fig. 6). We assume that the incident beams $A_u$ and $A_v$ are orthogonally polarized, so that their interference can be neglected.

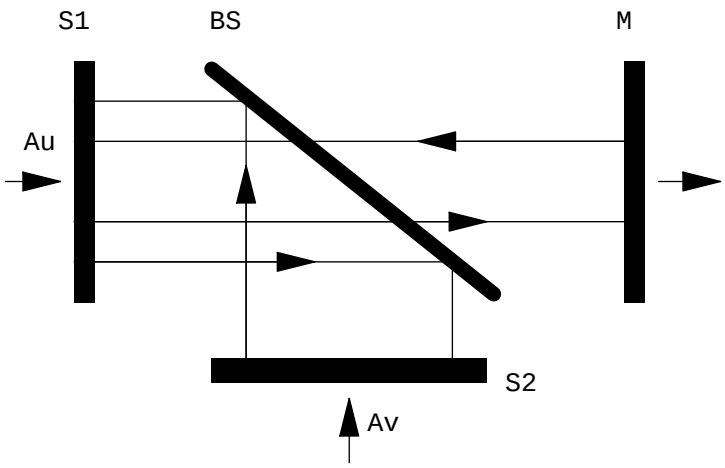


Figure 6: A scheme of the two-component system comprising the nonlinear elements S1 and S2, a mirror M, and a beam splitter BS.

The basic equations are obtained [18] as a generalization of the model (23) of a single-slice system:

$$\begin{aligned} \dot{u} + u - \nabla^2 u &= I_1 |\mathcal{D}(L_1) e^{iu}|^2 + I_2 |\exp(-i\nabla^2) e^{iv}|^2, \\ \tau \dot{v} + v - \delta^2 \nabla^2 v &= \kappa I_1 |\mathcal{D}(L_2) e^{iu}|^2, \end{aligned} \tag{45}$$

Here $u$ and $v$ denote the nonlinear phase modulation introduced by the first and the second slice, respectively; $\delta^2, \tau$ denote the material diffusivity and the characteristic relaxation time for second slice; the corresponding coefficients values for the first slice are normalized to unity by rescaling. The coefficients $I_j,\ (j = 1, 2)$, are proportional to the intensities of the corresponding incident beams; $\kappa$ is the ratio of the nonlinear sensitivities of the two slices. The model (45) describes the free space propagation in the same way as Eq. (23), and is also valid under assumption that the material response time is much larger than the round-trip time in the cavity.

The stationary homogeneous solution of Eq. (23), $u_0 = I_1 + I_2,\ v_0 = \kappa I_1$, loses stability when the input intensity exceeds a certain critical level. If $I_1$ is chosen as the bifurcation parameter, the linear analysis [18] defines the neutral curves for the Turing instability

$$I_1 = I_s(q) = \frac{(1 + \delta^2 q^2)(1 + q^2)}{2(1 + \delta^2 q^2) \sin L_1 q^2 + 2\kappa I_2 \sin^2 L_2 q^2}, \tag{46}$$

and the wave instability:

$$I_1 = I_w(q) = \frac{1 + \tau + q^2(\tau + \delta^2)}{2 \sin L_1 q^2}. \tag{47}$$

If $q = q_w$ is the critical wavenumber corresponding to a minimum of $I_w(q)$, the frequency of the wave mode is defined as

$$\omega^2 = (1 + \delta^2 q_w^2) \left(1 + q_w^2 - 2 I_w(q_w) \sin L_1 q_w^2\right) - 4\kappa I_w(q_w) I_2 \sin^2 L_2 q_w^2. \tag{48}$$

The minima of the neutral curves (46, 47) are determined by transcendental equations, and cannot be found analytically. A degenerate point where both coincide, so that the Turing and wave modes are excited simultaneously, can be located numerically. The relative heights of the minima of the neutral curves may interchange following a slight shift of the distance $L_1$, as seen in Fig. 7.

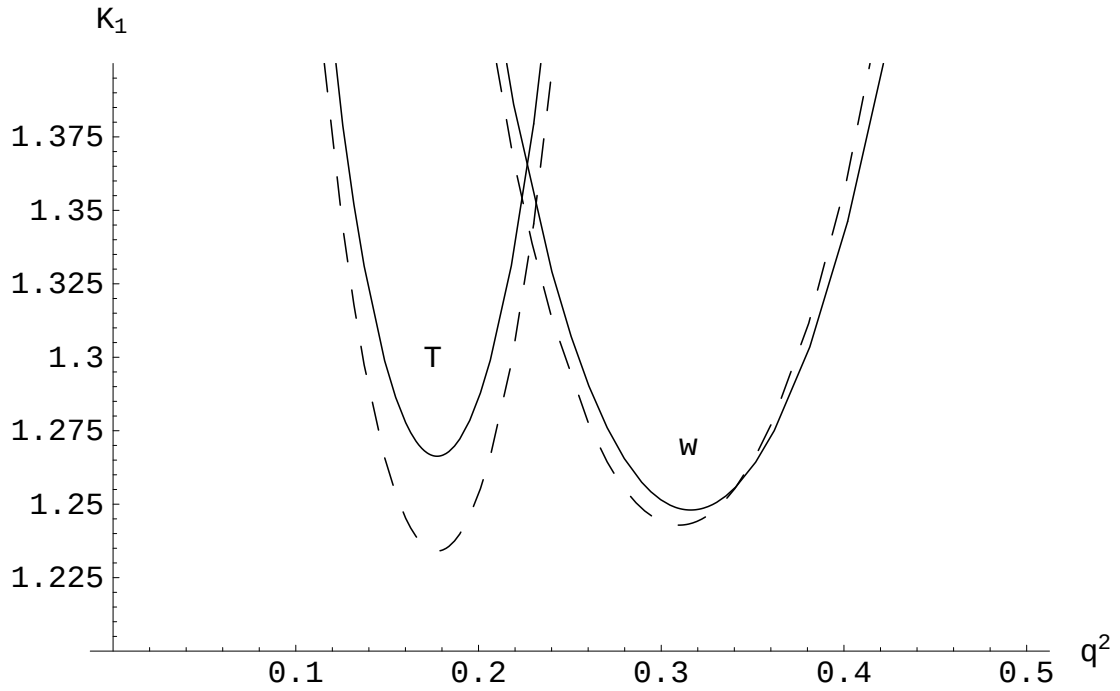


Figure 7: First positive branches of the neutral curves (46), corresponding to a Turing mode (T), and (47), corresponding to a composite wave mode (w), at $L_1 = 4.55$ (solid line) and $L_1 = 4.65$ (dashed line). The minima of the curves are interchanged by a small shift of the parameter. The values of other parameters are: $\tau = 1,\ L_2 = 1,\ I_2 = 1,\ \delta^2 = 0.5,\ \kappa = -4.5$.

### 4.2 Amplitude dynamics

A precursor of the wave–Turing resonance can be detected by constructing an amplitude equation under conditions when the minimum of the wave branch is slightly lower, as shown by solid lines in Fig. 7. For a wave bifurcation, the amplitude equation is obtained in the third order of the multiscale expansion (Section 2.1):

$$\dot{a}_j = \left[\mu + \nu_1|a_j|^2 + \sum_l \nu_2(\varphi_{jl})|a_l|^2\right] a_j, \tag{49}$$

where $\nu_2(\varphi_{jl})$ are interaction coefficients dependent on the angle $\varphi_{jl}$ between the $j$th and $l$th modes (we omit here resonant terms that appear when standing waves are included [11]). The angular dependence of Re $\nu_2(\varphi_{jl})$ shown in Fig. 8 has a sharp minimum. The vector sum of two modes at the angle corresponding to this minimum gives the weakly damped Turing mode at the minimum of the respective neutral curve. This indicates a near resonance when the levels of the two minima in Fig. 7 are close one to the other.

The simplest resonant structure at the degenerate bifurcation point includes two wave modes with the wavenumber $k$ and one Turing mode with the wavenumber $Q$ that both correspond to the minima of the respective neutral curves. The Fourier space structure is an isosceles triangle. The amplitude dynamics is described by Eqs. (10) where the coefficients are computed numerically with the help of our bifurcation package [19, 20].

This structure can be viewed as a basic building block of more complex structures rotationally invariant in the Fourier space. A single isosceles triangle structure in the Fourier space can

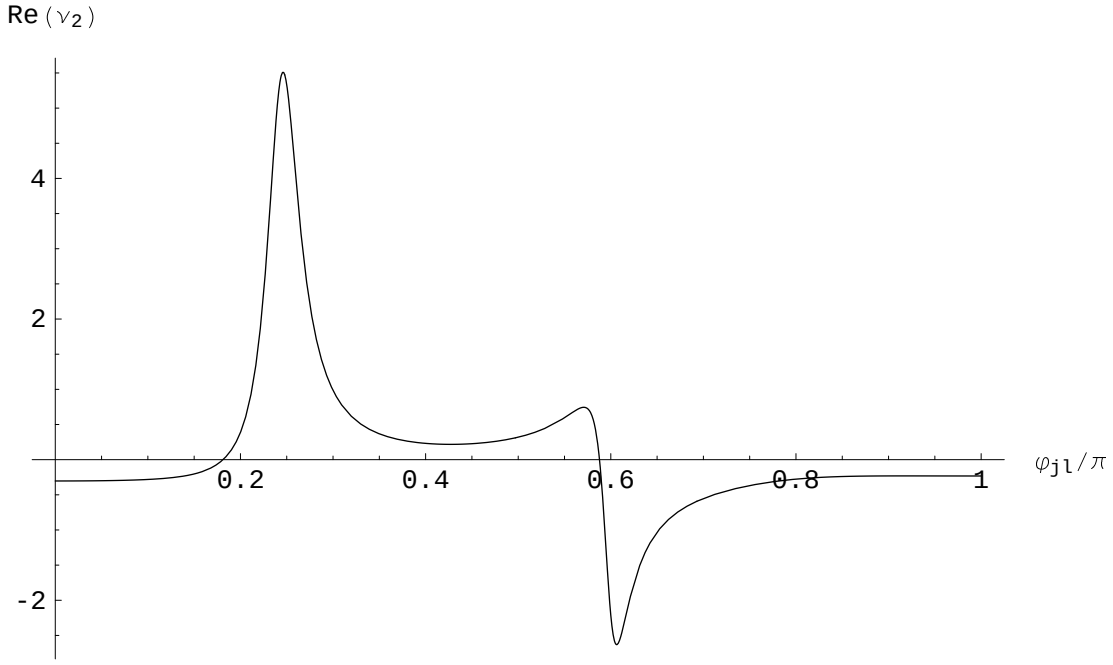


Figure 8: The angular dependence of the real part of the wave mode interaction coefficient $\nu_2(\varphi_{jl})$ calculated at $L_1 = 4.5,\ \tau = 1,\ L_2 = 1,\ I_2 = 1,\ \delta^2 = 0.5,\ \kappa = -4.5$.

be completed by one Turing and one wave modes in such a way that the new structure will be comprised of two isosceles triangles having one common side. Still more complicated structures can be constructed in a similar way.

The value of the acute angle between two wave modes in the triangle, which is determined by the ratio of the wavenumbers of the Turing and wave modes can be changed smoothly within a certain range by tuning the free parameter values. When the angle becomes commensurate with $\pi$, one can also envisage a closed rotationally invariant structure consisting of $2N$ isosceles triangles. Assuming that the amplitudes of all Turing modes are equal, $a_j^{(s)} = a$, and the amplitudes of wave modes are equal alternatingly, $a_{2n}^{(w)} = b,\ a_{2n+1}^{(w)} = c$, we arrive at the same dynamical system (10) with the only replacement $\nu_w \to 2\nu_w$. This means that the dynamics is similar for both cases. Since, unlike the case considered in Section 3, rotationally invariance is not compulsatory here, selection of either periodic or quasicrystalline pattern hinges upon weaker quadruplet interactions.

An example of a periodic orbit is seen in Fig. 9. A few snapshots of a quasicrystalline structure with $N = 4$ taken during the oscillation cycle are shown in Fig. 10. A square pattern in one of snapshots is observed when one couple of wave modes becomes nearly extinct; at this moment of time, the resonance breaks down, which triggers a sharp change of all variables, and the quasicrystalline structure is recovered.

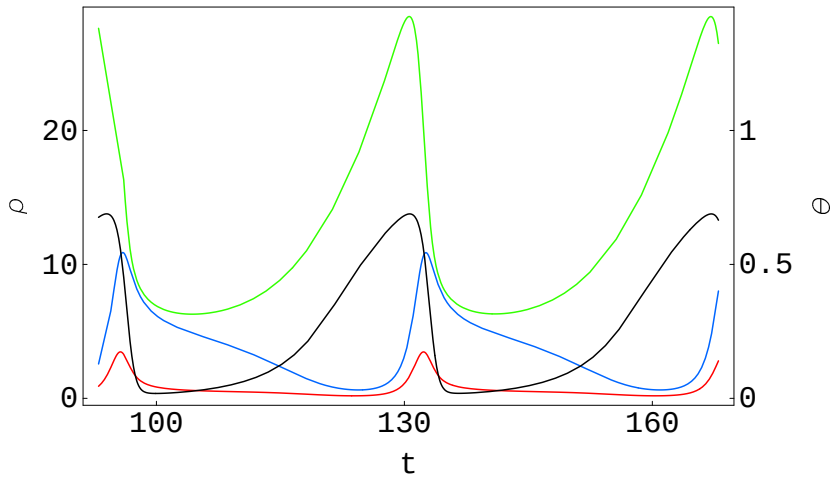


Figure 9: An asymmetric periodic solution of the system Eq. (12) at $\mu_w/\mu_s = -0.0238$, $\nu_s = 0.0678$, $\nu = 0.3523$, $\alpha = -0.66\pi$. Two periods are shown. The wave modes have different amplitudes which both undergo sharp oscillations. Oscillations of the Turing mode have the smallest amplitude, and the same period.

## 5 Conclusion

The nonlinear optical feedback systems considered in this communication have versatile and easily controllable dynamics. Complex small-amplitude patterns near a symmetry-breaking bifurcation point, that are very difficult to construct in other pattern-forming non-equilibrium systems, appear here in a very natural way. The central and, to our knowledge, novel point of this study is a primary role of resonant interactions between wave and Turing modes that facilitates formation of quasicrystalline structures, and allows dynamic confinement to the small amplitude region dominated by the action of triplet interactions only.

This research has been supported in part by the EU TMR network "Nonlinear dynamics and statistical physics of spatially extended systems".

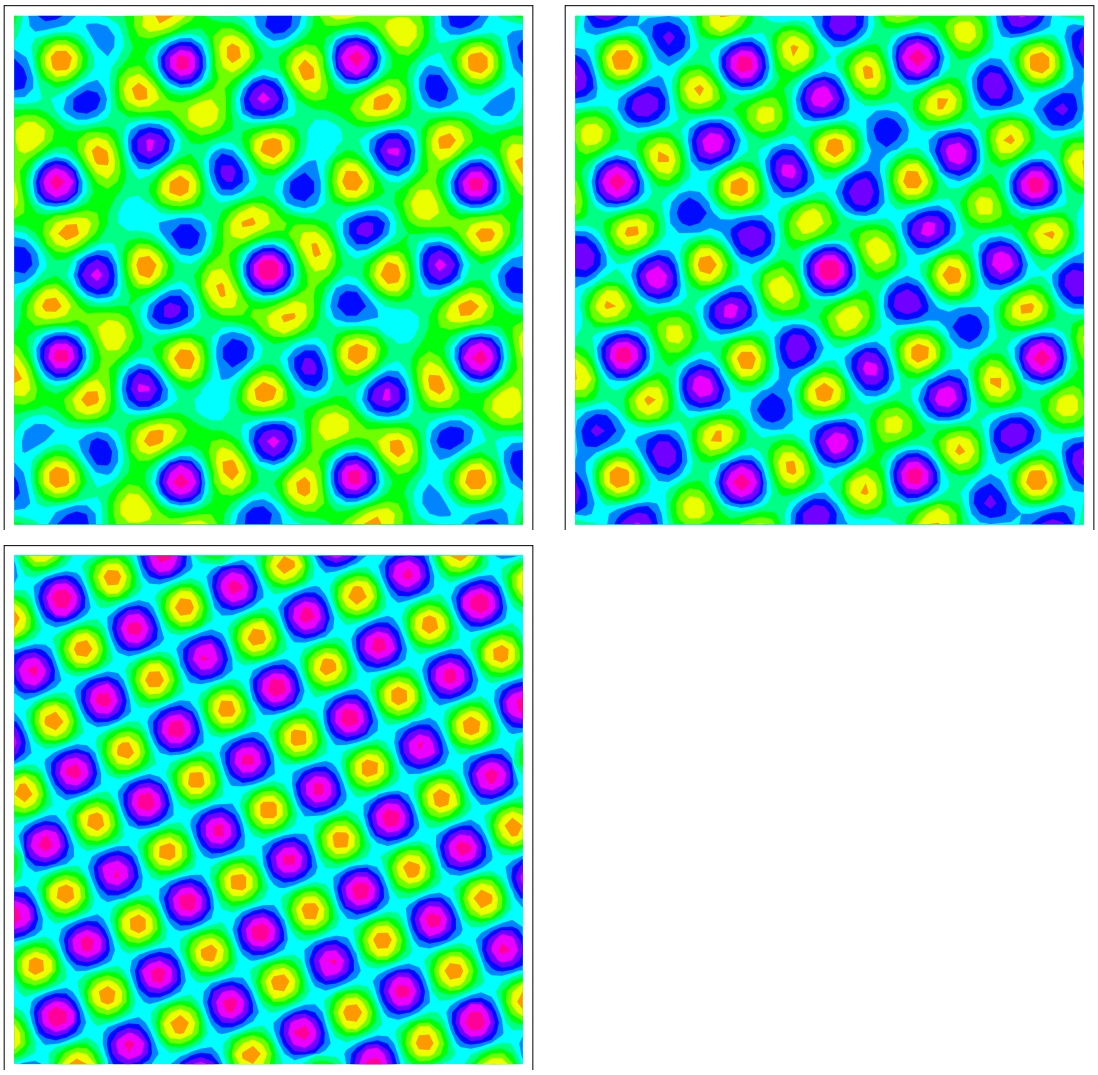

Figure 10: Snapshots taken during the oscillation cycle are shown in Fig. 9.

## References


[1] M. C. Cross and P. C. Hohenberg, Pattern formation outside equilibrium, Rev. Mod. Phys. **65**, 851 (1993).

[2] D. Walgraef, *Spatio-Temporal Pattern Formation*, Springer, New York (1996).

[3] S. Alexander and J. McTague, Should all crystals be bcc? Landau theory of solidification and crystal nucleation, Phys. Rev. Lett. **41** 702 (1978).

[4] L.M.Pismen, Symmetry breaking and pattern selection. Ch.2 in *Nonlinear dynamics*, ed.V.Hlavacek, Gordon & Breach, 1985.

[5] B.A. Malomed, A.A. Nepomnyashchy, and M.I. Tribelsky, Two-dimemional quasiperiodic structures in noneqilibrium systems, Zh. Eksp. Teor. Fiz. **96**, 684 (1989)

[6] B. Christiansen, P. Alstrom, and M.T. Levinsen, Ordered capillary wave states; quasicrystals, hexagons and radial waves, Phys. Rev. Lett. **68** 2157. (1992).

[7] W.S. Edwards and S. Fauve, Parametrically excited quasicrystalline surface waves, Phys. Rev. **E 47** R788 (1993).

[8] H.W. Müller, Model equations for two-dimensional quasipatterns, Phys. Rev. **A49** 1273 (1994).

[9] W. Zhang and J. Vinals, Square patterns and quasipatterns in weakly damped Faraday waves, Phys. Rev. **E 53**, R4283 (1996)

[10] A.A. Golovin, A.A. Nepomnyashchy, and L.M. Pismen, Pattern selection in long-scale Marangoni convection with deformable interface, Physica **D81** 117 (1995).

[11] L.M. Pismen, Bifurcation into wave patterns and turbulence in reaction-diffusion equations, Phys. Rev. **A23**, 334 (1981).

[12] S.A. Akhmanov, M.A. Vorontsov, V.Yu. Ivanov, A.V. Larichev, and N.I. Zelenykh, Controlling transverse-wave interactions in nonlinear optics: generation and interaction of spatiotemporal structures, JOSA **B9**, 78 (1992).

[13] E. Pampaloni, S. Residori, and F.T. Arecchi, Roll-hexagon transition in Kerr-like experiment, Europhys. Lett., **24**, 647 (1993).

[14] E. Pampaloni, P.L. Ramazza, S. Residori, and F.T. Arecchi, Two-dimemional crystals and quasicrystals in nonlinear optics, Phys. Rev. Lett., **74**, 258 (1995).

[15] S. Residori, P.L. Ramazza, E. Pampaloni, S. Boccaletti, and F.T. Arecchi, Domain coexistence in two-dimemional optical patterns, Phys. Rev. Lett., **76**, 1063 (1996).

[16] E. Pampaloni, S. Residori, S. Soria, and F.T. Arecchi, Phase locking in nonlinear optical patterns, Phys. Rev. Lett., **78**, 1042 (1997).

[17] D. Leduc, M. Le Berre, E. Ressayre, and A. Tallet, Quasipatterns in a polarization instability, Phys. Rev. **A52** 1072 (1996).

[18] E.V. Degtiarev and V. Watagin, Stability analysis of a two-component nonlinear optical system with 2-D feedback, Optics Comm. **124**, 309 (1996).

[19] L.M.Pismen, B.Y.Rubinstein, and M.G.Velarde, On automated derivation of amplitude equations in nonlinear problems, Int. J. of Bifurcations and Chaos, **6** 2163, 1996.

[20] L.M.Pismen and B.Y.Rubinstein, Tools for Nonlinear Analysis: I. Unfolding of Dynamical Systems, preprint chao-dyn/9601017, available at http://xxx.lanl.gov.

[21] A.C. Newell and J.V. Moloney, *Nonlinear Optics*, Addison - Wesley (1992).

[22] W.R. Firth, Spatial instabilities in a Kerr medium with single feedback mirror, J. of Modern Optics **37**, 151 (1990).